Oral presentation | Aero-acoustics
Aero-acoustics-II
Mon. Jul 15, 2024 2:00 PM - 3:30 PM Room B

[2-B-03] Aeroacoustic Study of Morphed Trailing-Edge Airfoils Using Large-Eddy Simulations

Donghun Kang[1], *Seongkyu Lee[1] (1. University of California, Davis)

Keywords: Trailing-Edge Noise, Large Eddy Simulations, Morphed Airfoils

**Twelfth International Conference on
Computational Fluid Dynamics (ICCFD12),
Kobe, Japan, July 14-19, 2024**

Aeroacoustic Study of Morphed Trailing-Edge Airfoils Using Large-Eddy Simulations

D. Kang* and S. Lee*
Corresponding author: skulee@ucavis.edu
* Department of Mechanical and Aerospace Engineering,
University of California, Davis, USA.

Abstract:
This paper leverages large-eddy simulations to study the impact of trailing-edge morphing on airfoil noise at a chord-based Reynolds number of 6×10^5, a Mach number of 0.088, and an angle of attack of 4°. A NACA 0018 airfoil is symmetrically morphed into two distinct shapes: concave (M1) and convex (M2) configurations. Turbulent flows are enforced using boundary-layer tripping near the leading edge. The Ffowcs Williams and Hawkings acoustic analogy is employed to radiate surface pressure fluctuations into the far field. The M1 airfoil demonstrates superior aeroacoustic performance compared to the baseline, while the M2 airfoil amplifies low-frequency noise, resulting in an increase in overall sound pressure level (OASPL). Although the M1 airfoil exhibits a lower OASPL than the baseline, it generates excessive noise in the high-frequency range. This contrasts with the M2 airfoil, which reduces high-frequency noise despite the increase in OASPL. The intrinsic noise generation and propagation mechanisms for both morphed airfoils, relative to the baseline, are delineated by analyzing the strength of the wall-pressure spectrum and performing modal analysis.

Keywords: Computational Fluid Dynamics, Aeroacoustics, Trailing-Edge Noise, Large-Eddy Simulations, Morphed Airfoils

1 Introduction

Trailing-edge noise from airfoils arises from the interaction between turbulent flows and a sharp edge [1, 2]. This noise occurs in various engineering applications, including aircraft wings, small-to-mid-scale unmanned aerial vehicles, and wind turbines. In particular, this noise has recently received significant attention as it has been identified as a primary noise source for emerging urban air mobility aircraft [3, 4, 5]. A key objective within the aeroacoustic community is to effectively reduce trailing-edge noise. Efforts to develop quieter vehicles have included implementing porous materials, morphing flaps, swept airfoils, and saw-tooth geometries on trailing edges [6, 7, 8]. Although these methods have achieved some degree of noise reduction, their effectiveness is often frequency-limited, and they may maintain overall sound pressure levels comparable to those of clean airfoils. Additionally, these approaches can result in trade-offs, such as compromised aerodynamic performance.

This study introduces a novel morphed trailing-edge design to investigate the impact of surface morphing on trailing-edge noise. We model concave and convex morphed trailing edges on a NACA 0018 airfoil using the PARFOIL airfoil design code [9, 10, 11]. The acoustic noise sources within turbulent boundary-layer flows are captured through wall-resolved large-eddy simulations (LES) and subsequently radiated to the far field via the Ffowcs Williams–Hawkings (FW–H) acoustic analogy. Spectral processing and modal analysis are employed to elucidate the sound production and propagation mechanisms attributable to the localized morphing effect.

2 Technical Approach

In this study, a NACA 0018 airfoil configuration is employed, subjected to a freestream with a Mach number of 0.088 and an angle of attack of 4°, at a chord-based Reynolds number of 6×10^5. The computational domain is modeled using structured meshes comprising 91 million cells. Boundary-layer tripping is implemented at 12.5% of the airfoil from the leading edge to enforce flow transition. The rhoPimpleFoam solver [12] is utilized to compute the compressible Navier-Stokes equations, while the wall-adapting local eddy-viscosity (WALE) model [13] is employed for sub-grid scale closure. Detailed

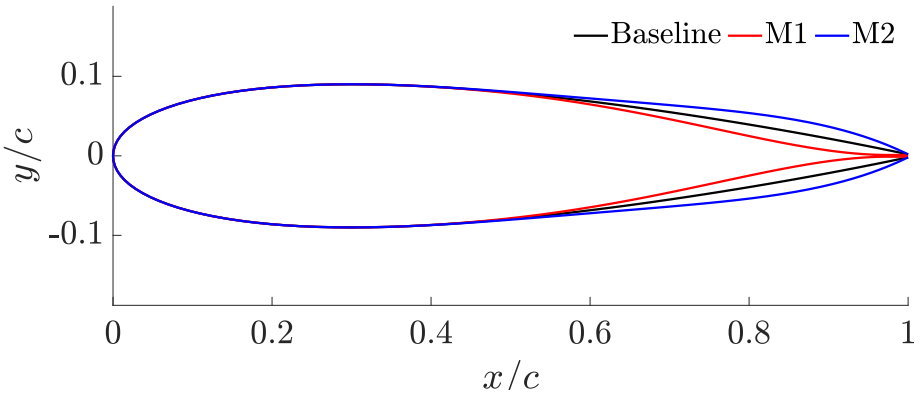

Figure 1: Infographic of baseline, M1, and M2 airfoil geometries.

boundary conditions over the computational domain used in this work are described and used for airfoil noise predictions in Refs. [14, 15, 16, 17]. The in-house acoustic code, PSU-WOPWOP [18, 19], is used to compute the Ffowcs Williams and Hawkings (FW-H) equation [20], and hydrodynamic pressure fluctuations are obtained from the airfoil surface. The local curvature of the airfoil is modified using the PARFOIL airfoil design code [9, 10, 11]. The first modified shape, designated as M1, features a boat-tail angle of $-15°$ with a measurement location at 0.9 in a symmetric manner between the upper and lower sides. The second shape, M2, mirrors M1's design but with an opposite boat-tail angle. Figure 1 illustrates both the baseline and the two morphed airfoil geometries. Note that the M1 airfoil exhibits concave morphing, whereas the M2 airfoil demonstrates convex morphing, starting from $x/c \approx 0.6$.

3 Results

The one-third octave band sound pressure level (SPL) is predicted using the FW-H acoustic analogy for the baseline and two morphed airfoils, as shown in Fig. 2. The sound receiver is placed 10 chord lengths above the trailing edge at midspan. The SPL is A-weighted to approximate the human ear's sound-filtering process. For the M1 airfoil, an acoustic benefit is observed up to 2.5 kHz compared to the baseline airfoil, although it emits slightly higher noise at very low frequencies between 0.2 and 0.3 kHz. A high-frequency acoustic penalty is noted; however, the overall sound pressure level (OASPL) of the M1 airfoil is estimated to be 1.2 dB less than that of the baseline airfoil, demonstrating superior aeroacoustic performance. In contrast, the M2 airfoil emits significantly more noise at low frequencies up to about 0.6 kHz, but the sound spectra beyond 0.6 kHz are lower than those of the baseline, which is a contrasting trend compared to the M1 airfoil. Nevertheless, the low-frequency amplification degrades the acoustic performance of the M2 airfoil relative to the baseline, resulting in a 2.6 dB increase in OASPL.

We extend the acoustic analysis using microphone arrays arranged in a circle with a radius of $10.0c$ to

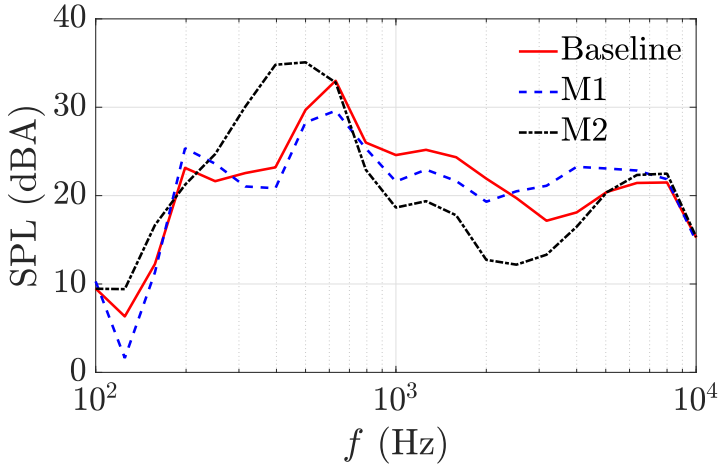

Figure 2: A-weighted one-third octave band SPLs for the baseline, M1, and M2 airfoils.

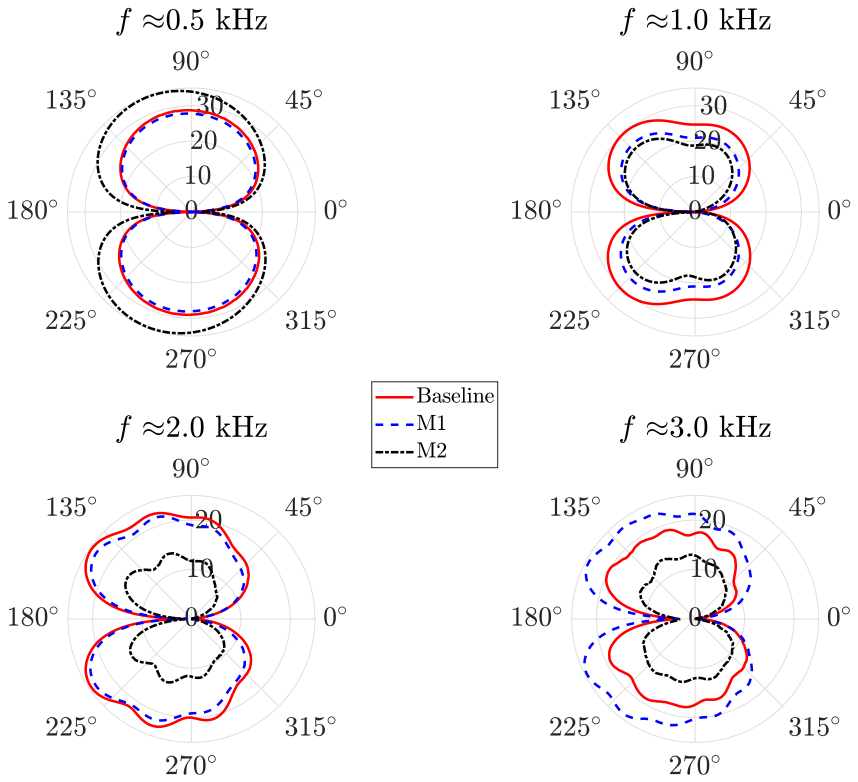

Figure 3: Directivity plots at four selected frequencies for the baseline, M1, and M2 airfoils.

examine the directional attributes of each airfoil's noise. Polar plots measured at midspan for four selected frequencies are provided in Fig. 3. The morphing effects do not appear to influence the directivity shape when compared to the baseline configuration, consistently transitioning from the compact dipole to the non-compact source with multiple lobes as frequency increases. However, the relative noise difference between the baseline and morphed airfoils is notable in the upstream direction, approximately θ=90-150°, specifically at 0.5 kHz and 3 kHz. Nonetheless, the aeroacoustic performance of the two morphed airfoils at $\theta = 90°$ remains consistent across varying azimuthal angles.

To identify the noise source, the wall-pressure spectrum (WPS) is calculated across the entire upper surface of the airfoil since WPS is a primary source of trailing-edge noise [21, 22]. The strength of the WPS for the baseline and two morphed airfoils at particular frequencies is displayed in Fig. 4. For the baseline airfoil, as shown in Fig. 4(a), turbulent streaks characterized by intermittent potent pressure fluctuations are observed across the surface under the turbulent boundary layer flows [23].

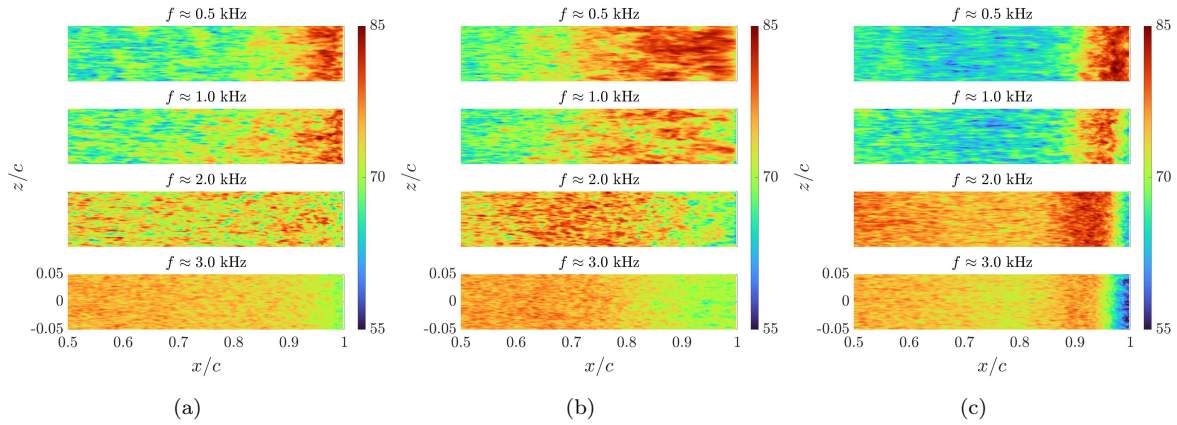

Figure 4: Contours of wall-pressure spectra at four selected frequencies for (a) baseline, (b) M1, and (c) M2 airfoils.

Additionally, strong hydrodynamic pressure sources near the trailing edge are observed at 0.5 kHz and 1 kHz. These formations may be attributed to the influence of large-scale turbulent eddies affected by the adverse pressure gradient (APG) and trailing-edge bluntness. For the M2 airfoil, the low-frequency amplification, as previously observed in Fig. 2, is distinctly identified in the WPS distribution at 0.5 kHz. This implies a significant influence of the convex shape on low-frequency noise, notably in the vicinity of the trailing edge. It is worth noting that the WPS strength appears to decrease abruptly near the trailing edge with increasing frequency, potentially leading to a favorable effect on noise reduction. However, radiation efficiency cannot be directly measured from this WPS contour, limiting the ability to quantify trailing-edge scattering influenced by the curvature morphing. Another observation is the wider strong WPS in the streamwise direction on the M1 airfoil's surface compared to the baseline at 0.5 kHz. This primarily results from the APG effect caused by the diverging shape starting at about $x/c \approx 0.6$, as shown in Fig. 1. This trend persists up to 1 kHz, while the WPS distributions at 2 kHz and 3 kHz are similar to those of the baseline airfoil. However, the lower scattering efficiency for the M1 airfoil at 0.5-1 kHz, as observed in Figs. 2 and 3, contrasts with these wider strong WPS distributions. This accentuates the necessity of systematically connecting the strength of the presented acoustic source with

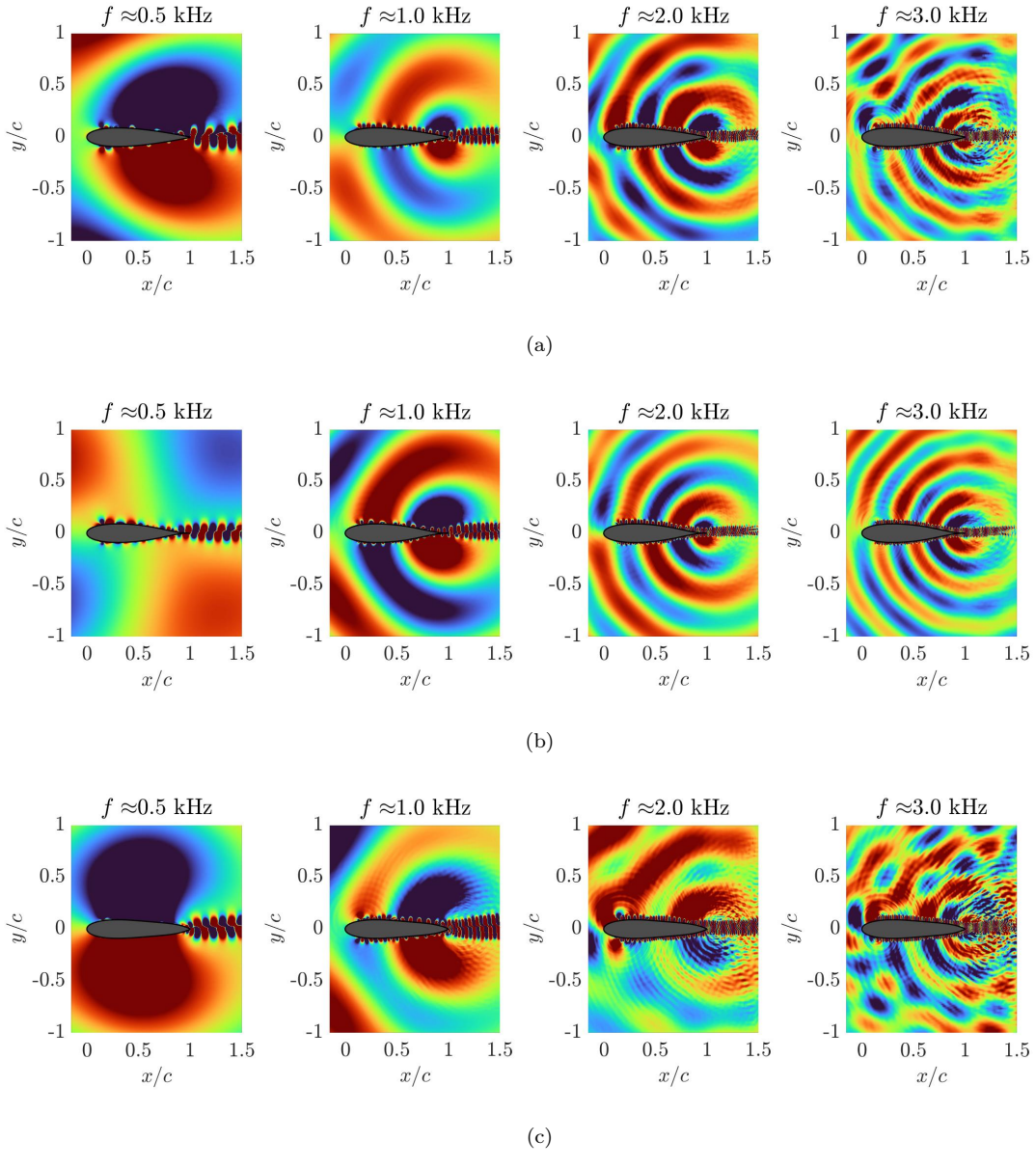

Figure 5: Contours of leading SPOD modes at four selected frequencies for (a) baseline, (b) M1, and (c) M2 airfoils.

the radiation efficiency, propagation pattern, and other acoustic dynamics, such as phase interference.

To examine sound propagation, the spatiotemporal coherent structure based on the spanwise-averaged pressure signal is extracted using spectral proper orthogonal decomposition (SPOD) [24, 25]. Figure 5 shows the contours of the leading SPOD modes for the baseline, M1, and M2 airfoils at specific frequencies. The color scale is saturated to clearly visualize the sound propagation, with blue indicating the lowest values and red indicating the highest values of the SPOD mode. The baseline airfoil typically shows a dipolar shape originating from the trailing edge with an opposite phase [26, 27], representing an acoustic discontinuity between the upper and lower sides of the airfoil. As frequency increases, the sound waves become acoustically non-compact sources, where the acoustic wavelength is shorter than the source length or airfoil chord. The M1 airfoil shows a less compact dipole pattern at 0.5 kHz while maintaining the acoustic discontinuity. This lower radiation efficiency aligns with the reduced SPL, as presented in Fig. 2. Notably, clearer noise propagation in the M1 airfoil at 3 kHz indicates more efficient radiation compared to the baseline and M2 airfoils, consistent with the increased SPL observed in Figs. 2 and 3. In contrast, the M2 airfoil exhibits inefficient radiation at higher frequencies, which could be linked to the rapid reduction in WPS strength near the trailing edge, as illustrated in Fig. 4. This observation suggests that, although the thicker airfoil created by the convex shape amplifies low-frequency noise, it could be utilized to reduce noise at relatively higher frequencies.

4 Conclusion

This work examined the impact of trailing-edge morphing on airfoil broadband noise using LES at a chord-based Reynolds number of 6×10^5, a Mach number of 0.088, and an angle of attack of 4°. The baseline NACA 0018 airfoil was symmetrically morphed using the boat-tail angle parameter in the PARFOIL airfoil design code, creating concave (M1) and convex (M2) configurations. The M1 airfoil exhibited better acoustic performance than the baseline, despite generating extra noise in the high-frequency band. The concave shape, representing a diverging curve, contributed to the enhanced WPS strength at 0.5 kHz and 1 kHz, but it did not lead to a noise penalty in terms of OASPL. Conversely, the M2 airfoil's thicker bluntness amplified the low-frequency noise, degrading overall acoustic efficiency despite reducing noise at high frequencies. Additional analyses focused on near-wall flow and acoustic interaction are required to reveal the mechanisms of noise generation, propagation, and reduction. As a future research topic, an optimized morphed airfoil can be designed to minimize sound levels across all frequency ranges. To complete the study, the aerodynamic performance of the morphed airfoils should be evaluated against the baseline configuration.

References

[1] N. Curle. The influence of solid boundaries upon aerodynamic sound. *Proc. R. Soc. A: Math. Phys. Eng. Sci.*, 231(1187):505–514, 1955.

[2] J. E. Ffowcs-Williams and L. H. Hall. Aerodynamic sound generation by turbulent flow in the vicinity of a scattering half plane. *J. Fluid Mech.*, 40:657–670, 1970.

[3] S. Li and S. Lee. Prediction of rotorcraft broadband trailing-edge noise and parameter sensitivity study. *J. Am. Helicopter Soc.*, 65:042006, 2020.

[4] S. Li and S. Lee. Prediction of urban air mobility multi-rotor vtol broadband noise using ucd-quietfly. *J. Am. Helicopter Soc.*, 66:032004, 2021.

[5] S. Li and S. Lee. Acoustic analysis and sound quality assessment of a quiet helicopter for air taxi operations. *J. Am. Helicopter Soc.*, 67:032001, 2022.

[6] S. Lee, L. Ayton, F. Bertagnolio, S. Moreau, T.P. Chong, and P. Joseph. Turbulent boundary layer trailing-edge noise: theory, computation, experiment, and application. *Prog. Aerosp. Sci.*, 126:100737, 2021.

[7] H. K. Jawahar, S. S. Vemuri, and M. Azarpeyvand. Aerodynamic noise characteristics of airfoils with morphed trailing edges. *Int. J. Heat Fluid Flow*, 93:108892, 2022.

[8] D. Kang and S. Lee. Numerical and analytical investigations on airfoil noise reduction with a sweep angle. In *30th AIAA/CEAS Aeroacoustics Conference*, Rome, Italy, June 4-7, 2024.

[9] J. W. Lim. Application of parametric airfoil design for rotor performance improvement. In *44th European Rotorcraft Forum*, Netherlands, Sept, 2018.

[10] C. Liu and S. Lee. Parametric airfoil design and sensitivity analysis for turbulent boundary layer trailing-edge noise reduction. *AIAA J.*, 60(4):2324–2341, 2022.

[11] J. Shum and S. Lee. Computational study of airfoil design parameters and sensitivity analysis for dynamic stall. *AIAA J.*, 62(4):1611–1617, 2024.
[12] H. G. Weller, G. Tabor, H. Jasak, and C. Fureby. A tensorial approach to computational continuum mechanics using object-oriented techniques. *Comput. Phys.*, 12(6), 1998.
[13] F. Nicoud and F. Ducros. Subgrid-scale stress modelling based on the square of the velocity gradient tensor. *Flow Turbul. Combust.*, 62:183–200, 1999.
[14] D. Kang, S. Lee, D. Brouzet, and S. K. Lele. Wavelet-based pressure decomposition for airfoil noise in low-mach number flows. *Phys. Fluids*, 35(7), 2023.
[15] D. Kang and S. Lee. A revisit of Amiet's trailing-edge noise theory through large-eddy simulations. In *AIAA Aviation Forum, San Diego, CA, AIAA Paper 2023–3629*. American Institute of Aeronautics and Astronautics, 2023.
[16] D. Kang and S. Lee. Aerodynamic and aeroacoustic effects of different transition mechanisms on an airfoil. *AIAA J.*, 62(4):1517–1535, 2024.
[17] D. Kang and S. Lee. Cross-spectrum method for acoustic source identification and visualization of airfoil noise. *Aerosp. Sci. Technol.*, 151:109278, 2024.
[18] K. S. Brentner, G. A. Bres, G. Perez, and H. E. Jones. Maneuvering rotorcraft noise prediction: A new code for a new problem. In *American Helicopter Society Aerodynamics, Acoustics, and Test and Evaluation Technical Specialist Meeting*, San Francisco, CA, Jan 23–25, 2002.
[19] S. Lee, K.S. Brentner, F. Farassat, and P.J Morris. Analytic formulation and numerical implementation of an acoustic pressure gradient prediction. *J. Sound Vib.*, 319(3-5):1200–1221, 2009.
[20] J. E. Ffowcs Williams and D. L. Hawkings. Sound generated by turbulence and surface in arbitrary motion. *Philos. Trans. R. Soc., A*, 264(1151):321–342, 1969.
[21] S. Lee. Empirical wall-pressure spectral modeling for zero and adverse pressure gradient flows. *AIAA J.*, 56(5):1818–1829, May 2018.
[22] S. Lee and J.G. Shum. Prediction of airfoil trailing edge noise using empirical wall pressure spectrum models. *AIAA J.*, 57(3):888–897, March 2019.
[23] J. Jiménez. Near-wall turbulence. *Phys. Fluids*, 25(10):101302, 2013.
[24] A. Towne, O. T. Schmidt, and T. Colonius. Spectral proper orthogonal decomposition and its relationship to dynamic mode decomposition and resolvent analysis. *J. Fluid Mech.*, 847:821–867, 2018.
[25] O. T. Schmidt and T. Colonius. Guide to spectral proper orthogonal decomposition. *AIAA J.*, 58(3):1023–1033, 2020.
[26] M. Wang, J. B. Freund, and S. K. Lele. Computational prediction of flow-generated sound. *Annu. Rev. Fluid Mech.*, 38:483–512, 2006.
[27] G. Desquesnes, M. Terracol, and P. Sagaut. Numerical investigation of the tone noise mechanisms over laminar airfoils. *J. Fluid Mech.*, 591:155–182, 2007.